SINTEF
PROCEEDINGS 6

14th International Conference on CFD in
Oil & Gas, Metallurgical and Process Industries
SINTEF, Trondheim, Norway, October 12–14, 2020

Proceedings from the 14th International Conference on CFD in Oil & Gas, Metallurgical and Process Industries

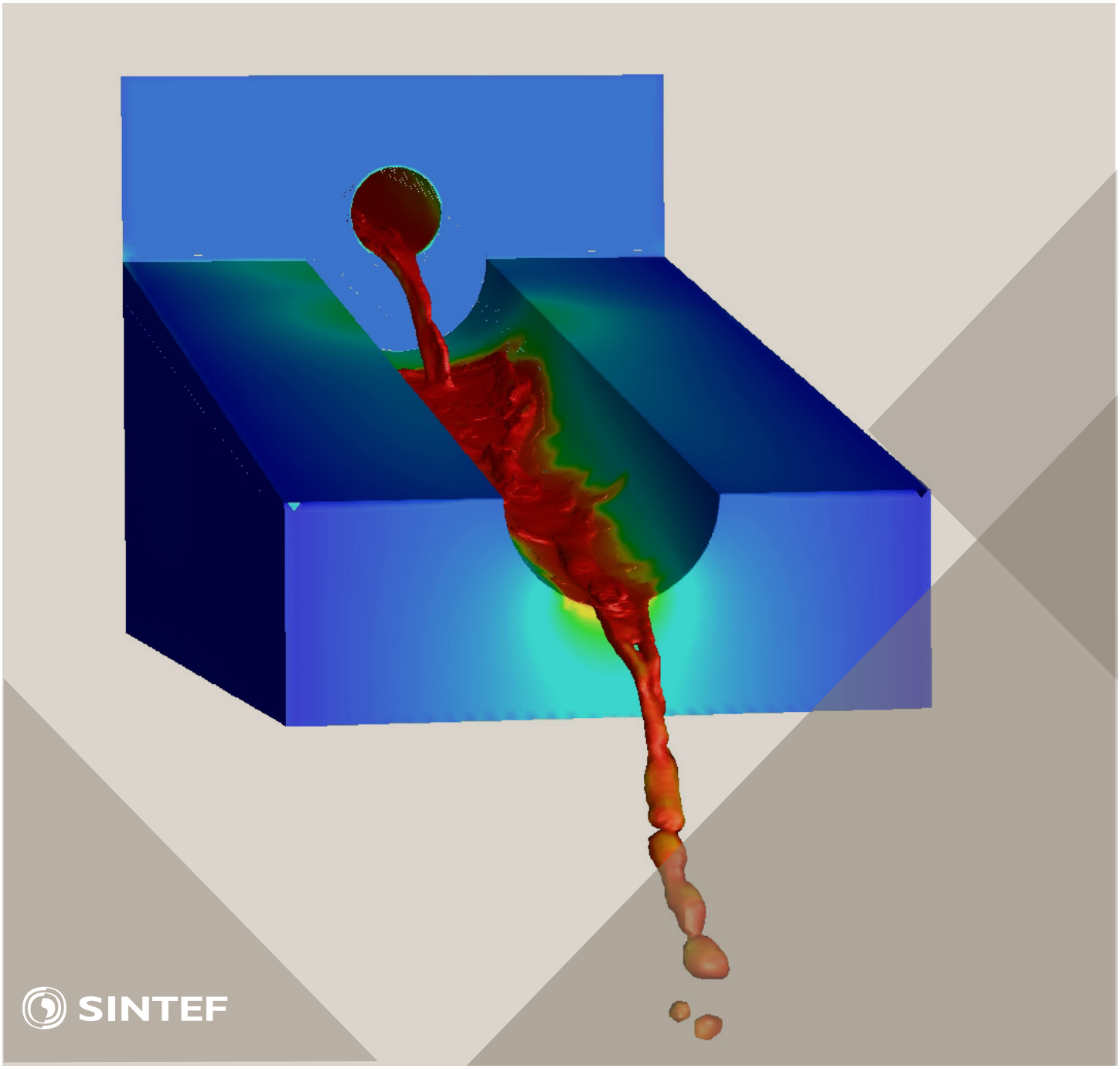

SINTEF Proceedings

Editors:
Jan Erik Olsen, Jan Hendrik Cloete and Stein Tore Johansen

Proceedings from the 14th International Conference on CFD in Oil & Gas, Metallurgical and Process Industries

SINTEF, Trondheim, Norway
October 12–14, 2020

SINTEF Academic Press

SINTEF Proceedings 6
Editors: Jan Erik Olsen, Jan Hendrik Cloete and Stein Tore Johansen

Proceedings from the 14th International Conference on CFD in Oil & Gas, Metallurgical and Process Industries, SINTEF, Trondheim, Norway, October 12–14, 2020

Keywords:
CFD, fluid dynamics, modelling

Cover illustration: Tapping of metal by Jan Erik Olsen

ISSN 2387-4295 (online)
ISBN 978-82-536-1684-1 (pdf)

SINTEF Academic Press
Address: Børrestuveien 3
PO Box 124 Blindern
N-0314 OSLO
Tel: +47 40 00 51 00

www.sintef.no/community
www.sintefbok.no

14th International Conference on CFD in Oil & Gas, Metallurgical and Process Industries
SINTEF, Trondheim, NORWAY
October 12-14 , 2020

DIRECT NUMERICAL SIMULATION OF MASS TRANSFER FROM A SINGLE BUBBLE VIA AN IMPROVED SUBGRID SCALE MODEL

Claire M.Y. CLAASSEN[1*], **Shafiul ISLAM**[1], **E.A.J.F. PETERS**[1], **Niels G. DEEN**[2], **J.A.M. KUIPERS**[1], **Maike W. BALTUSSEN**[1†]

[1]Multiphase Reactors Group, Department of Chemical Engineering and Chemistry, Eindhoven University of Technology, Eindhoven, The Netherlands

[2]Power and Flow Group, Department of Mechanical Engineering, Eindhoven University of Technology, Eindhoven, The Netherlands

[*] E-mail: c.m.y.claassen@tue.nl
[†] E-mail: m.w.baltussen@tue.nl

ABSTRACT

Hydrogenation, oxidation and alkylation are just some of the processes which are performed in bubble columns. One of the reasons to use a bubble column for these processes is the high interfacial mass transfer coefficients. Trying to simulate the mass transfer around the bubbles is however challenging due to the typically high Schmidt numbers of liquids, meaning that the mass boundary layer is very thin compared to the momentum boundary layer. To resolve this thin mass boundary layer, a subgrid scale model can be used. This work focuses on improving the subgrid scale model that we have embedded in our in-house front tracking framework of Claassen et al., AIChe J 2019. In the current implementation the unphysical numerical back diffusion at the grid into the bubble has been prevented with a staircase immersed boundary implementation. A verification has been performed by comparing the simulated, local and global Sherwood number with the analytical solution in creeping and potential flow regimes. Furthermore, the model was validated for 20 free rising bubbles of different shapes at industrial relevant Schmidt numbers (10^3-10^5). The model was able to correctly predict the Sherwood numbers.

Keywords: Computational Fluid Dynamics, bubble columns, Front Tracking, mass transfer, subgrid scale modeling, boundary layer, Direct Numerical Simulation .

NOMENCLATURE

Greek Symbols

δ	Boundary layer thickness, $[m]$
γ	Strain rate ($-\frac{\partial u_n}{\partial n^2}$), $[1/s]$
κ	Viscosity ratio
ρ	Density, $[kg/m^3]$
$\boldsymbol{\tau}$	Stress tensor, $[kg/ms^2]$
θ	Angle from the top of the bubble to the bottom, $[rad]$

Latin Symbols

c	Concentration, $[kg/m^3]$
D	Diffusion coefficient, $[m^2/s]$
$\mathbf{F}$	Force density, $[kg/m^2s^2]$
$\mathbf{g}$	Gravity constant, $[m/s^2]$
M_0	Total mass density in the model boundary layer region of a marker, $[kg/m^2]$
n	Normal coordinate from the interface, $[m]$
p	Pressure, $[kg/ms^2]$
Pe	Peclet number, $[-]$
Re	Reynolds number, $[-]$
Sh	Sherwood number, $[-]$
t	Time, $[s]$
$\mathbf{u}$	Velocity, $[m/s]$

Sub/superscripts

δ_0	At the model boundary layer thickness
σ	Surface tension
n	Normal direction from the interface
0	Model/bubble

INTRODUCTION

Bubbly flows are frequently encountered in many industries such as in the metallurgical, biochemical and chemical industry. In these industries, the bubbles are used to introduce mixing and/or supply reactants or remove reaction products. The efficiency of the last two processes depends on the mass transfer characteristics which are not thoroughly understood in bubbly flows. One of the reasons is the high Schmidt numbers typically found in gas-liquid systems. As the Schmidt number is high, the mass boundary layer is very small compared to the momentum boundary layer making it difficult to capture experimentally and to resolve numerically. Nevertheless, the subject has still been heavily studied in the past two decades.

For numerical studies, four different techniques have been used to resolve the boundary layer. The first technique uses the same uniform grid for solving the momentum equation and the advection-diffusion equation which ensures an easy coupling between the two equations. The disadvantage, however, is that both equations are solved with the grid size that is required to resolve the smallest boundary layer of the two. With this approach Bothe *et al.* (2004); Bothe and Warnecke (2005); Onea *et al.* (2009); Alke *et al.* (2009) and Hayashi and Tomiyama (2011) studied the mass transfer from single (deformable) bubbles, Taylor bubbles or bubble trains. Because the computational costs are high in this approach, several simplifications are made: the Schmidt number was kept low (Onea *et al.*, 2009; Alke *et al.*, 2009), an axisymmetric domain was used (Bothe *et al.*, 2004; Bothe and Warnecke, 2005; Alke *et al.*, 2009; Hayashi and Tomiyama, 2011), and/or the simulations were performed in 2D (Bothe and Warnecke, 2005; Alke *et al.*, 2009; Hayashi and Tomiyama, 2011).

The disadvantage of this first technique is reduced when two separate grids are used. The two grids are uniform and regular but have the size required for resolving the boundary layer of

the solved field. Since both grids are regular and uniform, interpolating the value of one grid to the other grid is still easy. With this technique, Davidson and Rudman (2002) investigated the mass transfer of deformable bubbles. Koynov *et al.* (2005) and Radl *et al.* (2007, 2008) also investigated the mass transfer of deformable bubbles with this technique, but they included a reaction. Whereas these studies used 2D domains, Darmana *et al.* (2006) simulated a single bubble in full 3D, but with a low Schmidt number of unity. Roghair *et al.* (2016) simulated a bubble swarm in 3D with the Schmidt number equal to unity.

This second technique only refines the field which requires refinement. However, refinement is only required at specific locations. The most important location is the boundary layer at the interface (although the concentration wake might also benefit from refinements). The refinement at the interface can be imposed by unstructured grids or techniques such as Adaptive Mesh Refinement (AMR). Unstructured grids have been used by Jung and Sato (2001, 2005); Dani *et al.* (2006); Wylock *et al.* (2011); Colombet *et al.* (2013); Deising *et al.* (2016) and Hayashi and Tomiyama (2011). Most of these researches simulated fixed bubble shapes due to the difficulty of moving the unstructured mesh with the bubble oscillations. Panda *et al.* (2020) showed the potential of AMR with simulations of forced-convection mass transfer from single bubbles at high Prandtl numbers ($\mathcal{O}(10^2)$). Mass transfer of moving deformable bubbles with industrial relevant Schmidt numbers in the range of $\mathcal{O}(10^3)$ - $\mathcal{O}(10^5)$ is however still a challenge, due to the high level of refinement that is required.

The last approach that is being used for the simulation of mass transfer from bubbles is different from the previous approaches. This approach does not resolve the boundary layer with a small enough grid size, but uses a subgrid scale (SGS) model to approximate the concentration boundary layer. So far two different SGS models for the mass transfer of bubbles have been developed. The Center of Smart Interfaces and the Institute for Mathematical Modeling and Analysis groups in Darmstadt have worked on a SGS model which is implemented in the Volume of Fluid framework. Their first model uses an analytical solution to the advection-diffusion equation which is simplified by assuming curvature effects to be negligible, convection to be dominant parallel to the interface and diffusion to be dominant tangential to the interface. The mass boundary layer thickness, used as a free model parameter, is then fitted from the simulation data and with that the convective and diffusive fluxes in interface cells are corrected (Alke *et al.*, 2010; Bothe and Fleckenstein, 2013; Gründing *et al.*, 2016; Weiner and Bothe, 2017). In one of the most recent publications, the analytical solution is no longer used. It is replaced by a solution provided by a machine learning method. With the result from the machine learning model the fluxes are corrected (Weiner *et al.*, 2019).

The other subgrid scale model has been developed at the University of Notre Dame by Aboulhasanzadeh *et al.* (2012). This subgrid scale model has been implemented in the Front Tracking (FT) framework. It makes use of the same assumptions as the other subgrid scale model to simplify the advection-diffusion equation. The advection-diffusion equation in a specific region normal to a FT marker is solved with an approximate boundary layer model. If the surface concentration in the boundary layer passes a certain threshold only then the mass is transferred to the grid that deals with the species transport in the remainder of the domain.

In this research, we chose to improve this latest model. First of all, we ensure species conservation in the SGS model during the crucial remeshing operations. Secondly, we make use of the exact analytical solution in the form of the error function instead of the second order polynomial that is used by Aboulhasanzadeh *et al.* (2012). And lastly, we prevent the numerical diffusion back into the bubble.

This article will first explain the details of the Front Tracking method. Next, the subgrid scale model and the made improvements will be elaborated on. Subsequently, the correctness of the improved model is shown with verification and validation of the method.

MODEL DESCRIPTION

Front Tracking

In Direct Numerical Simulations (DNS), two types of interface representations are encountered. The first are so-called front capturing methods in which the interface is not explicitly tracked but reconstructed from other quantities such as a color function for Volume of Fluid and a distance function for Level-Set. The second type are so-called front tracking methods in which the interface is explicitly tracked via Lagrangian points. One of these methods is the FT method in which the Lagrangian points are connected to form a closed triangular mesh. This method is used in this study.

In FT, the bubble moves by advecting the Lagrangian marker points with the local velocity, which is calculated via piecewise cubic spline interpolation of the Eulerian velocity field. As a result of the individual advection of the marker points, the mesh quality decreases. To correct this a remeshing algorithm is performed after the point positions are updated (Roghair *et al.*, 2016). When the distance between two marker points is too long and/or the edge shows local undulations, a point is added to give a high point concentration in curved parts (edge splitting). On the other hand, when the distance between two marker points is too short and/or the mesh is locally very flat, a point is removed which leads to a lower resolution in flat parts (edge collapsing). To ensure a good mesh quality (preferably equal lateral triangles), the connection between two markers might change from an edge between two points to an edge between the opposite two points (edge swapping). Lastly, to reduce the amount of remeshing operations that are needed all the marker points are evenly distributed over the interface while any volume changes due to the remeshing operations are corrected via the volume restoration/conservation method described by Kuprat *et al.* (2001) (edge smoothing). These crucial remeshing operations are graphically shown in Figure 1.

In FT, the Navier-Stokes equation and the continuity equation, given in equations 1 and 2, are then solved on a staggered Cartesian grid with a one-fluid formulation where the density is obtained via volume weighing averaging and the viscosity via harmonic averaging with the phase fraction.

$$\rho\frac{\partial \mathbf{u}}{\partial t} = -\nabla p - \rho\nabla\cdot(\mathbf{uu}) - \nabla\cdot\boldsymbol{\tau} + \rho\mathbf{g} + \mathbf{F}_\sigma \quad (1)$$

$$\nabla\cdot\mathbf{u} = 0 \quad (2)$$

The connection between the interface representation and the Cartesian grid is made via the surface tension force inside the incompressible Navier-Stokes equation. The surface tension is calculated at every FT marker as the sum of the tensile forces the marker exerts on its neighboring markers, i.e. the pull force method (Tryggvason *et al.*, 2001). This force is mapped to the nearby Eulerian cells using a mass-weighing function (Deen *et al.*, 2004).

To solve the equations, a projection-correction method is used to first solve for the velocity with equation 1 and then correct the velocity with equation 2. The convective term in the Navier-Stokes equation is discretized via a second order flux-delimited Barton scheme and treated explicitly. The diffusive term, on the other hand, is discretized using a second order central difference scheme and treated semi-implicit such that the velocities in all three directions can be solved separately. Further numerical details can be found in Dijkhuizen *et al.* (2010) and Roghair *et al.* (2016).

Mass Transfer

For the mass transfer, the advection-diffusion equation, given in equation 3, is solved on the same Cartesian grid as the hydrodynamics. The diffusion term is discretized with a second order central difference scheme and treated implicitly, while the convection term is discretized with the Van Leer scheme and treated explicitly. Since the SGS model deals with the mass transfer from the bubble interface to the liquid, the whole concentration field on the Eulerian grid is uniformly initialized to the initial concentration in the liquid. The concentration is assumed to not influence the fluid properties.

$$\frac{\partial c}{\partial t} + \mathbf{u} \cdot \nabla c = D \nabla^2 c \tag{3}$$

Subgrid-scale model

The subgrid-scale model describes the concentration profile close to the bubble interface, in a region of width δ_0, by means of a boundary layer approximation. The advection-diffusion equation in the boundary layer is simplified by assuming negligible curvature effects, dominant convection parallel to the interface and dominant diffusion tangential to the interface. Next to that, a Taylor expansion of the velocity is applied. This leads to the following simplified equation for each marker (Aboulhasanzadeh *et al.*, 2012):

$$\frac{\partial c}{\partial t} = n\gamma \frac{\partial c}{\partial n} + D \frac{\partial^2 c}{\partial n^2} \tag{4}$$

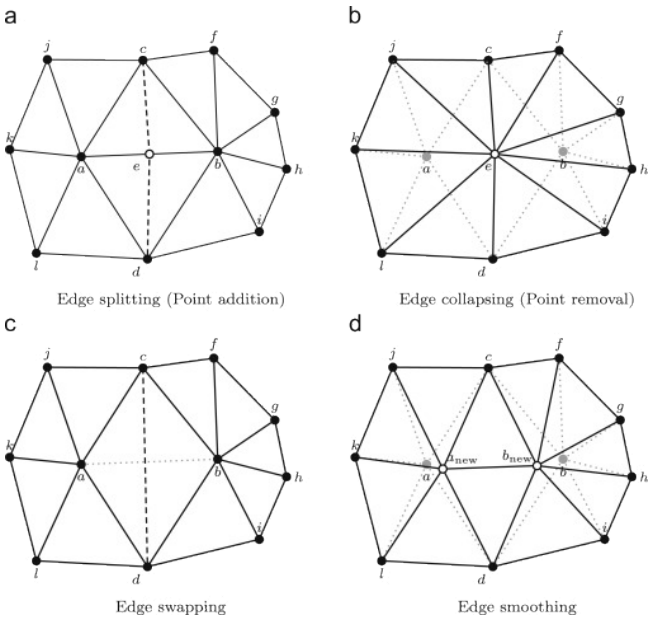

Figure 1: The remeshing operations that are used to maintain a good mesh quality.

The first term on the right hand side indicates the concentration change as a result of compression or expansion of the boundary layer due to the flow field and the second term indicates a concentration change as a result of diffusion normal to the interface.

Equation 4 is solved for every marker via the zeroth moment of the concentration in the model boundary layer region, i.e. $M_0 = \int_0^{\delta_0} c(n)\mathrm{d}n$. The evolution of the zeroth moment over time is given in equation 5.

$$\frac{dM_0}{dt} = -\gamma M_0 - D \left.\frac{\partial c}{\partial n}\right|_0 + \gamma c_{\delta_0} \delta_0 + D \left.\frac{\partial c}{\partial n}\right|_{\delta_0} \tag{5}$$

Aboulhasanzadeh *et al.* (2012) assumed a second order concentration profile to evaluate this equation explicitly. We will use the concentration profile given by the error function (equation 6). The concentration profile depends on the (real) boundary layer thickness (δ). When assuming a second order concentration profile the boundary layer thickness can easily be calculated from the total mass and the concentration profile. For the error function profile, this is however not the case as the error function can not be inverted. Therefore Newton-Rapson's method is used to calculate the real boundary layer thickness.

$$\frac{c(n)}{c_0} = \mathrm{erfc}\left(\sqrt{\pi}\frac{n}{\delta}\right) \tag{6}$$

The above given concentration profile only holds in the region close to the bubble interface. The Eulerian grid should solve the remainder of the concentration field. Note that equation 6 is the analytical solution of equation 4 for an semi-finite domain with concentration zero at infinity. As mentioned before the whole concentration field in initialized uniformly. The Eulerian grid only gets a concentration when the boundary layer thickness at a marker becomes larger than the model boundary layer thickness. When this happens the latter two terms in equation 5 are added to the Eulerian grid as a source term in equation 3 via polynomial weighing (Darmana *et al.*, 2006). There is a one-way coupling between the boundary layer SGS model and the bulk concentration field: the SGS model determines the molar flux into the fluid bulk, but the concentration in the bulk fluid does not influence the boundary layer development.

Remeshing

This subgrid scale model is implemented at the individual FT markers where the markers should store the mass density (M_0) to evaluate the change over time. When markers are removed, added or reshaped as a result of remeshing, the mass density of the changed markers should be adjusted accordingly to prevent numerical mass gain or loss. For every remeshing operation, we have implemented an algorithm to restore the total mass.

The first considered remeshing operation is edge splitting that occurs when an edge becomes too long and/or is not capable to capture the local curvature (Figure 1a). When an edge is split two markers are divided into two new markers each. These new markers will have the same mass density as the marker they originated from.

For edge swapping, a similar algorithm is used. With edge swapping two markers change how they are connected (Figure 1c). In this case, the average mass density is calculated and the mass density of both markers will be equal to this average after the remeshing.

For edge collapsing the algorithm is a little less straightforward as there are more markers involved. Edge collapsing is performed when an edge is too short and/or the local curvature is very low. This means the resolution can be reduced by removing an edge and hence removing two markers (Figure 1b). All the markers with one point connected to the to be removed edge will consequently change shape. To correct for the removed mass from the two markers the total mass before and after removal is calculated. The difference in mass is then distributed over all markers that have grown in size weighted by their size increase.

The last remeshing operation, edge smoothing, follows the same algorithm as for edge collapsing. Edge smoothing slightly changes the position of the two edge endpoints to yield a better local node distribution (Figure 1d). As a result, all markers that contain one of those nodes will slightly change in size, similar to what happens for edge collapsing. Hence the algorithm here is again: calculate the total mass before and after smoothing and distribute the difference over all involved markers that increased in size weighted by their size increase.

IBM

In our previous work (Claassen *et al.*, 2019) as well as in the work of Aboulhasanzadeh *et al.* (2012) an unphysical mass flux into the bubble was found. On the grid the convection-diffusion equation, equation 3, is solved using a one-fluid approximation. This means the concentration can diffuse from the fluid to the gas phase without a problem. A concentration gradient appears into the bubble at δ_0 when mass is transferred from the SGS model to the Eulerian grid on which the concentration inside the bubble is initialized to zero. A source is thus introduced close to the bubble interface resulting into a flux to the bubble. To prevent this flux, we have further improved the model by implementing an immersed boundary at the end of the boundary layer. At this boundary a Neumann boundary condition is enforced using a staircase Immersed Boundary Method (IBM) (Tseng and Ferziger, 2003; Mizuno *et al.*, 2015; Seo and Mittal, 2011) to prevent molar fluxes into the bubble. Before the IBM can be implemented, the cells that are outside the bubble and boundary layer region should be determined. Only to these cells, the source term from the SGS model should be forced.

To determine the cells outside the bubble and boundary layer region, we adopted the approach of Mittal *et al.* (2008) in which for every cell the vector to the closest marker is identified. The dot product of this vector and the marker's normal vector determines where the cell center is located. To take into account the mass boundary layer, the marker's center is temporary transposed a distance of δ_0 in its normal direction. Performing this procedure for every cell at every time step will result in quite some computational overhead. However, since markers move maximally one grid cell in one time step, the computational time can be reduced significantly by only considering the eight cells neighboring a marker.

To map the mass flux that comes out of the SGS model the polynomial weighing procedure Darmana *et al.* (2006) is slightly adapted. The flux is only mapped to the cells that lay outside the model boundary layer. The same polynomial weighing is used but corrected by the total weight of the cells that lay outside the boundary layer.

To prevent the unphysical flux into the bubble, the implicit matrix coefficients and the explicit source vector are adjusted for cells outside of the bubble and the boundary layer that have a neighbor inside the bubble or boundary layer and for all cells inside the bubble or boundary layer. This last step is not necessary but is expected to speed up the computation. For cells outside the bubble and boundary layer that have a neighbor inside the bubble or boundary layer the implicit diffusive flux between those cells are set to zero. The explicit convective flux, discretized with the Van Leer scheme, depends on four cells: the cell at which the flux is calculated (i), the neighboring cell on one side ($il = i - 1$) and the two neighboring cells on the other side ($ih = i + 1$, $ihh = i + 2$). In case the cell at which is being calculated (i) is inside the bubble or the boundary layer, the flux is set to zero. If the $i - 1$ cell is inside the bubble or the boundary layer, the flux is calculated with the concentration of i at the place of il. If ih is inside the bubble or the boundary layer, then the flux is set to zero. Lastly, if ihh is inside the bubble or the boundary layer, the flux is calculated with ih at the place of ihh. The procedure for il and ihh is analogous to the flux calculation when those cells would be outside of the domain. All cells inside the bubble or boundary layer are always forced to have a zero concentration (although this is not strictly necessary as the IBM will already prevent mass from going there).

RESULTS

Verification

To check the implementation of this new model we used a test where a bubble is placed in Stokes flow and a test where the bubble is placed in potential flow. For these tests the velocity field is not solved but imposed from the Hadamard-Rybczynski solution (Hadamard, 1911; Rybczynski, 1911) and Clift *et al.* (1978), respectively. Since we use a moving frame of reference (Deen *et al.*, 2004) the velocity and pressure field are only set at initialization. Further simulations settings are given in Table 1.

Table 1: Settings used for the verification tests.

Bubble diameter	3.2	mm
Bubble resolution	40	Grid cells
Domain size	$2.5 \times 2.5 \times 2.5$	d_e
Time step	0.000001	s
Simulation time	6.0	s
Viscosity ratio	0.185	-
Velocity	0.05	m/s
Peclet number	160,000	-

To verify the correct implementation the local and global Sherwood number obtained in the simulations are compared with the analytical solution. In the simulations the Sherwood number is calculated as $\frac{dc}{dn}\Big| = -\frac{2c_0}{\delta}$ at every marker. The analytical local and global Sherwood number are obtained from equation 7 and 8 for Stokes flow and equation 9 and 10 for potential flow.

$$\frac{Sh(\theta)}{\sqrt{Pe}} = \sqrt{\frac{3}{\pi}}\frac{1+\cos\theta}{\sqrt{2+\cos\theta}}\sqrt{\frac{1}{1+\kappa}} \quad (7)$$

$$\frac{Sh}{\sqrt{Pe}} = \sqrt{\frac{4}{3\pi}\frac{1}{1+\kappa}} \quad (8)$$

$$\frac{Sh(\theta)}{\sqrt{Pe}} = \sqrt{\frac{3}{\pi}}\frac{1+\cos\theta}{\sqrt{2+\cos\theta}}\sqrt{3} \quad (9)$$

$$\frac{Sh}{\sqrt{Pe}} = \sqrt{\frac{4}{\pi}} \quad (10)$$

In Figure 2, the computed local Sherwood number averaged over the last 2s of the Stokes flow simulation are plotted together with the analytical solution. Figure 3 shows the same

plot but for potential flow. For comparison, we also performed a simulation with our improved SGS model with the second order profile as described by Aboulhasanzadeh *et al.* (2012). The results of these simulations are also included in the graphs. As can be seen, in both cases our SGS model predicts the local Sherwood number correctly especially at the top of the bubble. At the bottom of the bubble, there's a small mismatch both with the erf function profile as well as with the second order profile. This is attributed to the fact that at the bottom of the bubble the model boundary layer is almost completely saturated which makes it difficult to correctly fit the concentration profile. Nevertheless, the global Sherwood number prediction is still accurate. With our SGS model with the error function, the Sherwood number was underestimated by 0.9% and 0.6% in Stokes flow and potential flow, respectively. This is almost half the error compared to the second order profile which overestimated the Sherwood number by 1.6% and 1.7%, respectively.

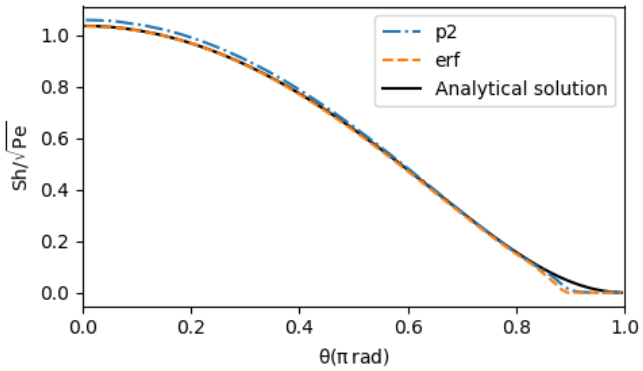

Figure 2: Local Sherwood number in the Stokes flow test. Averaged over the last 2s of the simulation.

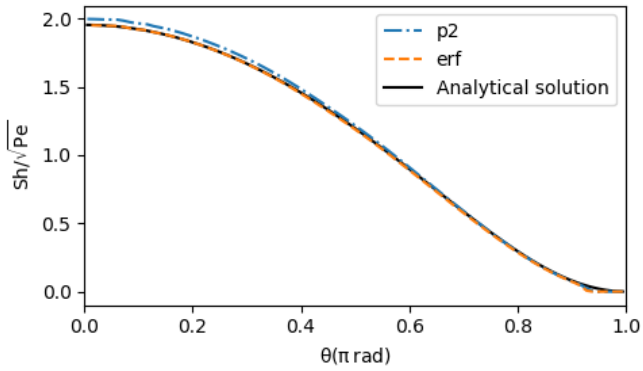

Figure 3: Local Sherwood number in the potential flow test. Averaged over the last 2s of the simulation.

Validation

To validate our code, we have performed the same set of simulations as in Claassen *et al.* (2019). The cases are indicated in the Grace diagram in Figure 4. The simulations have been performed with a moving frame of reference (Deen *et al.*, 2004). The simulations settings are the same as in our previous work and are summarized in Table 2.

Since the hydrodynamics of the code was already validated in Claassen *et al.* (2019), the focus here is only on the mass transfer. To validate the mass transfer the time-average global Sherwood number calculated from the simulations is compared with literature correlations. For spherical and slightly ellipsoidal bubbles the correlation of Takemura and Yabe (1998) (equation 11) and of Lochiel and Calderbank (1964) (equation 12) are used. For wobbling bubbles the correlation of Brauer and Mewes (1971) (equation 13) and of Anderson (1967) (equation 14) are used. The simulation results together with predictions from these correlations are shown in Figure 5 and Figure 6 for spherical/ellipsoidal bubbles and wobbling bubbles, respectively. For spherical/ellipsoidal bubbles the Sherwood number is always within 10% of the literature correlations that have an accuracy of 7% and 12% for Takemura and Yabe (1998) and Lochiel and Calderbank (1964) respectively. It may appear as if our simulations are constantly lower than the correlations, this is, however, due to the fact that our bubbles or not all perfectly spherical as the correlations assume. Figueroa-Espinoza and Legendre (2010) showed that for low Reynolds numbers ($<\sim 100$) the Sherwood number decreases with a slightly increased aspect ratio which supports our results. For the wobbling bubbles the accuracy is always within 15% of the literature correlations. For this regime the literature correlations mismatch between one another (this is even more visible in Claassen

Table 2: Simulations settings for the 20 cases depicted in Figure 4. Z is the domain height in the rise direction and is case dependent.

Bubble diameter	$1.5 - 6.9$	mm
Bubble resolution	20	Grid cells
Initial bubble shape	Spherical	
Domain size	$100 \times 100 \times Z$	Grid cells
Initial bubble position	$50 \times 50 \times 60$	%
Interface concentration (c_0)	1.0	kg/m^3
Time step	$10^{-6} - 10^{-5}$	s
Dimensionless simulation time	100	-
Viscosity ratio	$48 - 66$	-
Density ratio	$640 - 908$	-
Eötvos number	$0.2 - 60$	-
log Morton	$-11 - 1$	-

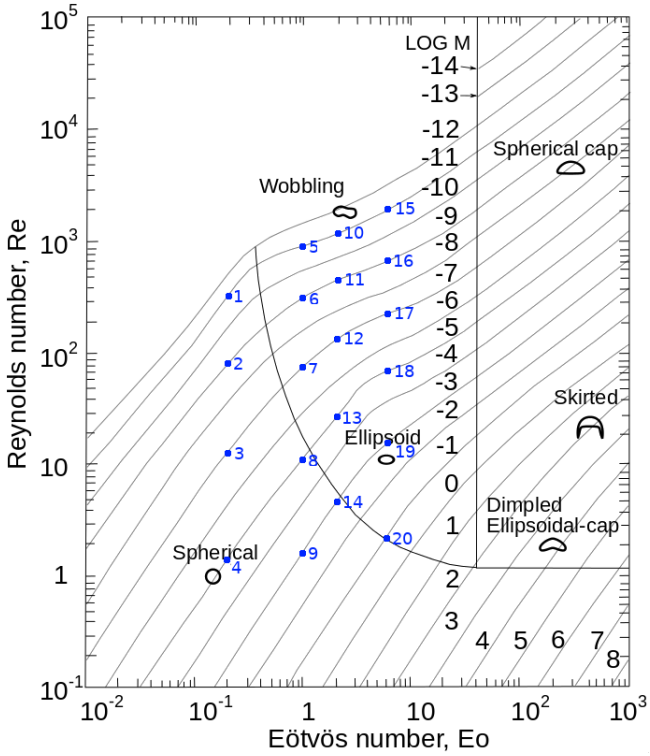

Figure 4: 20 simulations of different bubble shapes that have been performed.

et al. (2019) where more correlations are included), it is therefore harder to make a statement about the precise accuracy of our method.

$$Sh = \frac{2}{\sqrt{\pi}} \sqrt{1 - \frac{2}{3\left(1 + 0.09Re^{2/3}\right)^{3/4}}} \left(2.5 + \sqrt{Pe}\right) \quad (11)$$

$$Sh = \frac{2}{\sqrt{\pi}} \sqrt{Pe\left(1 - \frac{2+3\kappa}{1+\sqrt{\kappa\lambda}} \frac{1.45}{Re^{1/2}}\right)} \quad (12)$$

$$Sh = 2 + 0.015Re^{0.89}Sc^{0.7} \quad (13)$$

$$Sh = 1.2\sqrt{\frac{d_e f_N}{D}} \text{ with } f_N = d_e \sqrt{\frac{48\sigma}{\pi^2 d_e^3 \rho_l (2+3\lambda)}} \quad (14)$$

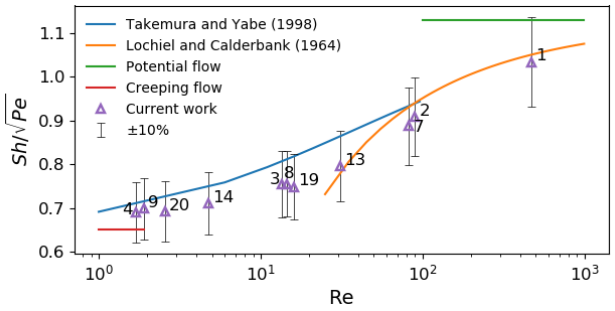

Figure 5: Calculated Sherwood number for the spherical/ellipsoidal cases (markers with errorbars) together with literature correlations (lines).

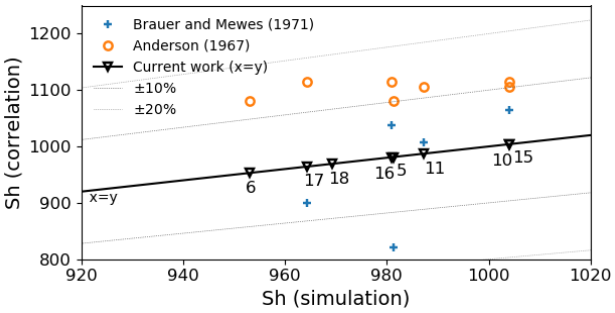

Figure 6: Calculated Sherwood number for the wobbling cases together with literature correlations.

The above-mentioned Sherwood results agree with the results of our previous work (Claassen *et al.*, 2019). The local concentration on the Eulerian grid, however, is different due to the here implemented IBM. Figure 7 shows the concentration on the grid with and without IBM for case 1. The figure shows the diffusion back into the bubble when IBM is not used, while the model with IBM clearly shows that there is no diffusion in the bubble. Due to the use of a log scale for the concentration, a difference in the wake predicted by the two models becomes visible. The wake of our new model has the expected thin shape, while the other wake is broader due to the diffusion back into the bubble and even outside the top of the bubble.

CONCLUSION

In this paper, the SGS model initially developed by Aboulhasanzadeh *et al.* (2012) is improved by including an algorithm for the SGS model upon remeshing, using the exact erf function and implementing an IBM to prevent numerical diffusion into the bubble. To check the implementation, the predicted Sherwood number of the model is verified for a bubble in Stokes flow and a bubble in potential flow. The computed Sherwood number was slightly under-predicted at the bottom of the bubble, but the global Sherwood number was still within 1% of the analytical solution. Furthermore, we validated the new model with 20 free rising bubbles. For the spherical and ellipsoidal bubbles, the Sherwood number deviated maximally 10% from literature correlations that mostly have an accuracy of roughly 10%. For the wobbling bubbles, the deviation was maximally around 15%, which is still good considering the accuracy of the correlations in this regime. We attribute the deviation between our results and the literature results to the fact that the correlations are rather strict and only applicable in very specific conditions such a potential or creeping flow and/or perfect sphericity. New, more broadly applicable correlations should be developed for which potentially this model could be used. Lastly, we compared the concentration profile on the grid predicted by a model with and without IBM implemented and found that the numerical diffusion into the bubble also leads to an incorrect wake which is broader than it should be. While the numerical diffusion into the bubble could be considered as negligible as is done in our previous work and the work of Aboulhasanzadeh *et al.* (2012), the broader wake is not neglectable.

REFERENCES

ABOULHASANZADEH, B., THOMAS, S., TAEIBI-RAHNI, M. and TRYGGVASON, G. (2012). "Multiscale computations of mass transfer from buoyant bubbles". *Chemical Engineering Science*, **75**, 456 – 467.

ALKE, A., BOTHE, D., KRÖGER, M., WEIGAND, B., WEIRICH, D. and WEKING, H. (2010). "Direct numerical simulation of high schmidt number mass transfer from air bubbles rising in liquids using the volume-of-fluid-method". *Ercoftac Bulletin*, **82**, 5–10.

ALKE, A., BOTHE, D., KROEGER, M. and WARNECKE, H.J. (2009). "Vof-based simulation of conjugate mass transfer from freely moving fluid particles". *Computational Methods in Multiphase Flow V*, 157–168.

ANDERSON, R.A. (1967). *Fundamentals of vibrations*. Macmillan.

BOTHE, D. and WARNECKE, H. (2005). "Vof-simulation of rising air bubbles with mass transfer to the ambient liquid".

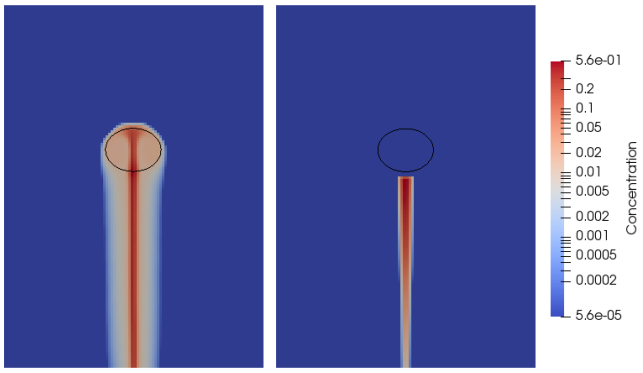

Figure 7: Slice of the concentration profile for case 1 with our previous work (Claassen *et al.*, 2019) without IBM (left) and our current work with IBM implemented (right). The black circle is the bubble contour.

10th Workshop on Transport Phenomena in Two-phase Flow, Bothe & Warnecke, Sunny Beach, Bulgaria, 61–72.

BOTHE, D. and FLECKENSTEIN, S. (2013). "A volume-of-fluid-based method for mass transfer processes at fluid particles". *Chemical Engineering Science*, **101**, 283 – 302.

BOTHE, D., KOEBE, M., PRUSS, J. and WARNECKE, H.J. (2004). "Direct numerical simulation of mass transfer between rising gas bubbles and water". *Sommerfeld, M. ed., Bubble Flows: Analysis, Modelling and Calculation*, 159–174.

BRAUER, H. and MEWES, D. (1971). *Stoffaustausch einschließlich chemischer Reaktionen*. Sauerländer.

CLAASSEN, C.M.Y., ISLAM, S., PETERS, E.A.J.F., DEEN, N.G., KUIPERS, J.A.M. and BALTUSSEN, M.W. (2019). "An improved subgrid scale model for front-tracking based simulations of mass transfer from bubbles". *AIChE Journal*.

CLIFT, R., GRACE, J.R. and WEBER, M.E. (1978). *Bubbles, drops and particles*. Academic Press, New York.

COLOMBET, D., LEGENDRE, D., COCKX, A. and GUIRAUD, P. (2013). "Mass or heat transfer inside a spherical gas bubble at low to moderate reynolds number". *International Journal of Heat and Mass Transfer*, **67**, 1096 – 1105.

DANI, A., COCKX, A. and GUIRAUD, P. (2006). "Direct numerical simulation of mass transfer from spherical bubbles: the effect of interface contamination at low reynolds numbers." *International Journal of Chemical Reactor Engineering*, **4**, A2.

DARMANA, D., DEEN, N.G. and KUIPERS, J.A.M. (2006). "Detailed 3D modeling of mass transfer processes in two-phase flows with dynamic interfaces". *Chemical Engineering & Technology*, **29**, 1027–1033.

DAVIDSON, M.R. and RUDMAN, M. (2002). "Volume-of-fluid calculation of heat or mass transfer across deforming interfaces in two-fluid flow". *Numerical Heat Transfer B*, **41**, 291–308.

DEEN, N.G., VAN SINT ANNALAND, M. and KUIPERS, J.A.M. (2004). "Multi-scale modeling of dispersed gas-liquid two-phase flow". *Chemical Engineering Science*, **59(8-9)**, 1853–1861.

DEISING, D., MARSCHALL, H. and BOTHE, D. (2016). "A unified single-field model framework for volume-of-fluid simulations of interfacial species transfer applied to bubbly flows". *Chemical Engineering Science*, **139**, 173–195.

DIJKHUIZEN, W., ROGHAIR, I., VAN SINT ANNALAND, M. and KUIPERS, J.A.M. (2010). "DNS of gas bubbles behaviour using an improved 3D Front Tracking model–model development". *Chemical Engineering Science*, **65(4)**, 1427–1437.

FIGUEROA-ESPINOZA, B. and LEGENDRE, D. (2010). "Mass or heat transfer from spheriodal gas bubbles rising through a stationary liquid". *Chem. Eng. Sci.*, **65**, 6296–6309.

GRÜNDING, D., FLECKENSTEIN, S. and BOTHE, D. (2016). "A subgrid-scale model for reactive concentration boundary layers for 3d mass transfer simulations with deformable fluid interfaces". *International Journal of Heat and Mass Transfer*, **101**, 476 – 487.

HADAMARD, J. (1911). "Movement permanent lent d'une sphere liquide et visqueuse dans un liquide visqueux". *Comptes Rendus*, **152**, 1735.

HAYASHI, K. and TOMIYAMA, A. (2011). "Interface tracking simulation of mass transfer from a dissolving bubble". *The Journal of Computational Multiphase Flows*, **3(4)**, 247–261.

JUNG, R.T. and SATO, T. (2001). "Direct numerical simulation on single-droplet flow with mass transfer". *Chem. Eng. Technol.*, **24**, 1071–1075.

JUNG, R.T. and SATO, T. (2005). "Numerical simulation of high schmidt number flow over a droplet by using moving unstructured mesh". *Journal of Computational Physics*, **203(1)**, 221–249.

KOYNOV, A., KHINAST, J.G. and TRYGGVASON, G. (2005). "Mass transfer and chemical reactions at dynamic interfaces". *AIChE J.*, **51**, 2786– 2800.

KUPRAT, A., KHAMAYSEH, A., GEORGE, D. and LARKEY, L. (2001). "Volume conserving smoothing for piecewise linear curves, surfaces, and triple lines". *Journal of Computational Physics*, **172**, 99–118.

LOCHIEL, A.C. and CALDERBANK, P.H. (1964). "Mass transfer in the continuous phase around axisymmetric bodies of revolution". *Chemical Engineering Science*, **19(7)**, 471–484.

MITTAL, R., DONG, H., BOZKURTTAS, M., NAJJAR, F.M., VARGAS, A. and VON LOEBBECKE, A. (2008). "A versatile sharp interface immersed boundary method for incompressible flows with complex boundaries". *Journal of computational physics*, **227(10)**, 4825–4852.

MIZUNO, Y., TAKAHASHI, S., NONOMURA, T., NAGATA, T. and FUKUDA, K. (2015). "A simple immersed boundary method for compressible flow simulation around a stationary and moving sphere". *Mathematical problems in Engineering*, **2015**.

ONEA, A., WÖRNER, M. and CACUCI, D.G. (2009). "A qualitative computational study of mass transfer in upward bubble train flow through square and rectangular minichannels". *Chemical Engineering Science*, **64(7)**, 1416–1435.

PANDA, A., PATEL, H., PETERS, E.A.J.F., BALTUSSEN, M.W. and KUIPERS, J.A.M. (2020). "A multiple resolution approach using adaptive grids for fully resolved boundary layers on deformable interfaces at high schmidt numbers". *Submitted to Chemical Engineering Science*.

RADL, S., TRYGGVASON, G. and KHINAST, J.G. (2007). "Flow and mass transfer of fully resolved bubbles in non-newtonian fluids". *AIChE journal*, **53(7)**, 1861–1878.

RADL, S., KOYNOV, A., TRYGGVASON, G. and KHINAST, J.G. (2008). "DNS-based prediction of the selectivity of fast multiphase reactions: Hydrogenation of nitroarenes". *Chem. Eng. Sci.*, **63**, 3279–3291.

ROGHAIR, I., VAN SINT ANNALAND, M. and KUIPERS, J.A.M. (2016). "An improved front-tracking technique for the simulation of mass transfer in dense bubbly flows". *Chemical Engineering Science*, **152**, 351–369.

RYBCZYNSKI, W. (1911). "Über die fortscheitende bewegung einer flüssigen kugel in einem zähllen medium". *Bull. Acad. Sci. Cracovie*, **A**, 40.

SEO, J.H. and MITTAL, R. (2011). "A sharp-interface immersed boundary method with improved mass conservation and reduced spurious pressure oscillations". *Journal of computational physics*, **230(19)**, 7347–7363.

TAKEMURA, F. and YABE, A. (1998). "Gas dissolution process of spherical rising gas bubbles". *Chemical Engineering Science*, **53(15)**, 2691 – 2699.

TRYGGVASON, G., BUNNER, B., ESMAEELI, A., JURIC, D., AL-RAWAHI, N., TAUBER, W., HAN, J., NAS, S. and JAN, Y.J. (2001). "A Front-Tracking method for the computations of multiphase flow". *Journal of Computational Physics*, **169(2)**, 708–759.

TSENG, Y.H. and FERZIGER, J.H. (2003). "A ghost-cell immersed boundary method for flow in complex geometry". *Journal of computational physics*, **192(2)**, 593–623.

WEINER, A. and BOTHE, D. (2017). "Advanced subgrid-scale modeling for convection-dominated species transport at fluid interfaces with application to mass transfer from rising bubbles". *Journal of Computational Physics*, **347**, 261–289.

WEINER, A., HILLENBRAND, D., MARSCHALL, H. and BOTHE, D. (2019). "Data-driven subgrid-scale modeling for convection-dominated concentration boundary layers". *Chemical Engineering & Technology*, **42(7)**, 1349–1356.

WYLOCK, C., LARCY, A., COLINET, P., CARTAGE, T. and HAUT, B. (2011). "Direct numerical simulation of bubble-liquid mass transfer coupled with chemical reactions: Influence of bubble shape and interface contamination". *Colloids ans Surfaces A: Physicochem. Eng. Aspects*, **381**, 130–138.